ACS OMEGA

http://pubs.acs.org/journal/acsodf

Article

Synthesis and Photoluminescence Properties of MoS_2/Graphene Heterostructure by Liquid-Phase Exfoliation

Durai Murugan Kandhasamy,* Paulpandian Muthu Mareeswaran, Selvaraju Chellappan, Dhenadhayalan Namasivayam, Afaf Aldahish, and Kumarappan Chidambaram

Cite This: *ACS Omega* 2022, 7, 629–637

Read Online

ACCESS | Metrics & More | Article Recommendations

ABSTRACT: Here, we report the synthesis of MoS_2/graphene heterostructure in single-stage, liquid-phase exfoliation using a 7:3 isopropyl alcohol/water mixture. Further, the synthesized heterostructure was characterized using UV−visible and micro-Raman spectroscopies, transmission electron microscopy (TEM), and dynamic light scattering (DLS) analysis. UV−visible and micro-Raman analyses confirmed that the synthesized heterostructure had mostly few-layered (two-to-four sheets) MoS_2. The photophysical properties of the heterostructure were analyzed using steady-state and time-resolved luminescence techniques. Enhanced photoluminescence was observed in the case of the heterostructure probably due to an increase in the defect sites or reduction in the rate of nonradiative decay upon formation of the sandwiched heterostructure. Applications of this heterostructure for fluorescence live-cell imaging were carried out, and the heterostructure demonstrated a better luminescence contrast compared to its individual counterpart MoS_2 in phosphate-buffered saline (PBS).

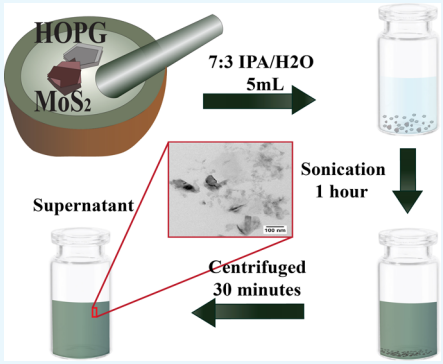

INTRODUCTION

Electronic and optical properties of atomically thin, two-dimensional (2D) layered graphene and transition metal dichalcogenides (TMDCs) have attracted significant interest due to their dependence on layer thickness and crystallite size.[1−6] The presence of unsaturated d-orbitals and chemically active edge sites makes them act as semiconductors, semimetals, ferromagnets, and even superconductors.[2] Specifically, the inherent properties of two-dimensional (2D) materials are altered with a decrease in layer numbers to a single layer or a few layers, making them promising candidates in various fields of science.[5,7−9] Moreover, these 2D materials show enhanced biosensing and catalytic applications owing to their large surface area.[6,10] In particular, graphene is a widely known 2D material, which has become the research focus due to its excellent mechanical, thermal, electrical, and optical properties and its high specific surface area since its discovery in 2004.[11−13] It has shown potential applications in biosensors, batteries, photovoltaics, and supercapacitor applications.[14] Unlike graphene, MoS_2 is a direct-band-gap semiconductor with tunable electronic properties as a function of layer thickness and size.[8,15,16] MoS_2 shows potential applications in photocatalysis, energy storage, bioimaging, and biosensor applications.[4,10,17−19] Lateral and vertical heterostructures of graphene and TMDCs have attracted much interest due to their improved performance and stability in various fields ranging from energy conversion to biomedical applications.[20−24] The characteristic, high-quality heterointerface strongly affects the built-in electric field and hence the charge transfer and dissociation of excitons. This results in the manipulation of the optical and electronic properties of 2D materials with improved performance toward specific applications in catalysis, sensing, and optoelectronic devices.[25−30]

Various methods have been proposed for the synthesis of high-quality heterostructures such as direct transfer of mechanically exfoliated materials, chemical vapor deposition, van der Waals epitaxy, and in situ catalytic growth using presynthesized precursor materials.[31−34] The large-scale synthesis of MoS_2/graphene composite by a hydrothermal method using Mo and S precursors in the presence of exfoliated graphene for electrocatalytic water splitting was reported by Pandey et al.[35] Also, there are several reports on the large-scale synthesis of composite-like materials of graphene with other 2D materials.[2,36,37] However, synthesizing vertical/lateral stacks of these 2D heterostructures with controlled size and purity on a large scale is challenging and very rarely reported in the literature.[34,38,39]

Liquid-phase exfoliation (LPE) using *N*-methylpyrrolidone (NMP) and other organic solvents is shown to produce various

Received: September 22, 2021
Accepted: December 21, 2021
Published: December 31, 2021

monolayer materials including graphene, hBN, MoS_2, WS, etc.[40−43] Moreover, LPE using water and other low-boiling organic solvents can efficiently produce defect-free nanosheets of 2D materials including monolayers in suspension by a wet chemical method, followed by ultrasonication and centrifugation. Recently, it has been reported that liquid-phase exfoliation (LPE) effectively produces dielectric nanosheets by probing and matching the surface tension components of comparatively low-boiling solvents.[44,45] Monolayer enriched, luminescent nanosheets of MoS_2 and WS_2 have been synthesized in single-stage liquid-phase exfoliation with varying percentages of water/isopropanol mixture, and a 3:7 combination exhibits an enhanced exfoliation for these dichalcogenides.[46,47]

The large-scale synthesis of quality heterostructures is challenging and in some cases, solvents used for exfoliation may also chemically modify these materials.[28,34,38] But, in this work, for the first time we have successfully synthesized the MoS_2/graphene heterostructure in a water/isopropyl alcohol solvent mixture via a scalable, single stage. Further, the method is benign to the environment and cost-effective compared to other methods reported. Thus, the synthesized material was characterized by spectroscopic techniques such as UV−visible and micro-Raman spectroscopies, and the structural aspects were probed using transmission electron microscopy (TEM) with small-angle electron diffraction (SAED) patterns. The luminescence properties were investigated by steady-state and time-resolved photoluminescence measurements. The applicability of this material toward live-cell imaging was studied, and better performance was observed for the heterostructure.

RESULTS AND DISCUSSION

UV−Visible and Micro-Raman Spectroscopic Analysis. The heterostructure of MoS_2/graphene and its individual counterparts MoS_2 and graphene suspensions was synthesized using MoS_2 and highly oriented pyrolytic graphite (HOPG) crystals as detailed in the Materials and Methods section (Figure 1). The UV−visible absorption spectra recorded for

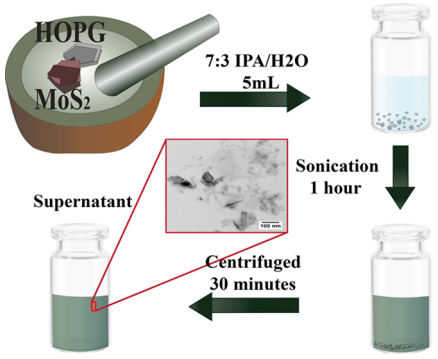

Figure 1. Synthesis of the MoS_2/graphene heterostructure via the liquid-phase exfoliation method.

the MoS_2/graphene heterostructure and its individual components exhibit the characteristic absorption bands of these materials. The absorption spectrum (Figure 2A, red) of exfoliated graphene in the IPA/H_2O mixture shows a peak at around 270 nm, tailing until the end of the measured spectral range. This reveals that the graphene sample has both thin-layered graphene and thick-multilayered ones. The signature absorption maxima due to the exciton states of MoS_2 was observed in the liquid-phase exfoliated MoS_2 and the MoS_2/graphene heterostructure at 430, 607, and 665 nm, and they are assigned to C, B, and A exciton states of molybdenum disulfide, respectively.[48] A detailed investigation on the effect of exfoliated sheet thickness and size on the absorption maximum of MoS_2 has been documented before.[5] The observed "A" exciton maximum at 665 nm in both MoS_2 and its heterostructure clearly indicates that the obtained suspension has mostly thin layers of one-to-four sheet thickness. The ratio between the normalized absorption low at ∼340 and B exciton maximum at 607 nm (OD_B/OD_{340}) gives us the lateral size and the concentration of the particles in the suspension.[5] Estimated ratios of 0.38 and 0.34 indicate a ∼200 nm lateral size for MoS_2 and MoS_2/graphene dispersions. These observations were further confirmed by particle size measurement using dynamic light scattering.

The particles dried and resuspended in MilliQ water were used for dynamic light scattering measurements, and the profile of the lateral size is shown in Figure 2B. The mean lateral size of the particles was found to be 243 ± 72 and 261 ± 93 nm for MoS_2 and the MoS_2/graphene heterostructure, respectively. This is again consistent with the estimated lateral size using UV−visible spectra of the sample as mentioned in the previous section. The lateral size of the particles depends on the nature of the exfoliating medium and ultrasonication time.[40] The lateral size observed is comparable to the previous report with a larger polydispersity index for MoS_2 alone under identical conditions.[46] Moreover, the synthesized heterostructure reveals an increase in lateral size and polydispersity index. This may be attributed to the formation of a heterostructure with varying dimensions and thicknesses. MoS_2 and the MoS_2/graphene heterostructure show a ζ-potential value of −59 and −62 mV, respectively. This indicates that the surfaces of the exfoliated materials are negatively charged. ζ-Potential of the exfoliated nanosheets of MoS_2 and graphene is known to be dependent on the pH of the solution.[49,50] Both show a wide range of ζ-potential values between +10 and −60 mV as a function of the pH of the solution. A value of around −50 mV was reported under neutral pH. In the present case, a slightly higher value of −63 mV was observed for the heterostructure. This shows that the nature of charge density does not change upon the formation of the heterostructure.

The Raman spectrum of the two-dimensional materials provides a wealth of information regarding the thickness, defects, and more specifically, the nature of the interaction between layers in the case of heterostructures. The Raman spectrum of liquid-phase exfoliated graphene exhibits peaks at 1347, 1575, 2444, and 2701 cm^{-1} assignable to D, G, D*, and 2D bands, respectively (Figure 3A). An intense D band observed in the Raman signal indicates an increase in defect sites leading to more number of sp^3-hybridized carbon atoms.[14] The heterostructure exhibits Raman features at 1340, 1571, 2434, and 2671 cm^{-1}. The peak positions are due to the same vibronic bands of graphene mentioned above with the shift in the peak positions toward lower wavenumbers. This shift may be due to the formation of the heterostructure, which in turn affects the out-of-plane vibrations. The integrated intensity ratio I_D/I_G for the D band and G band is widely used for characterizing the defect quantity in graphitic materials. The estimated values of the I_D/I_G ratio were 0.1970 and 0.3946 for exfoliated graphene and the MoS_2/graphene heterostructure, respectively.

https://doi.org/10.1021/acsomega.1c05250
ACS Omega 2022, 7, 629−637

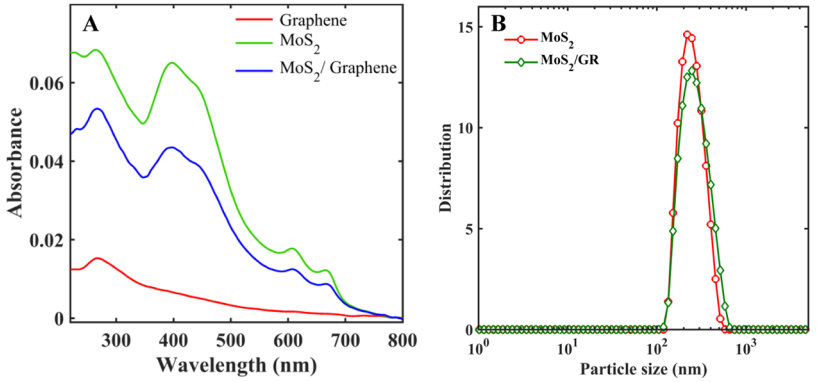

Figure 2. (A) UV−visible spectra of liquid-phase exfoliated graphene (red line), MoS_2 (green line), and the MoS_2/graphene (blue line) heterostructure in a 3:7 water/isopropanol mixture. (B) Lateral size histogram measured by dynamic light scattering of liquid-phase exfoliated MoS_2 (red line) and the MoS_2/graphene heterostructure (green line) in a 3:7 water/isopropanol mixture.

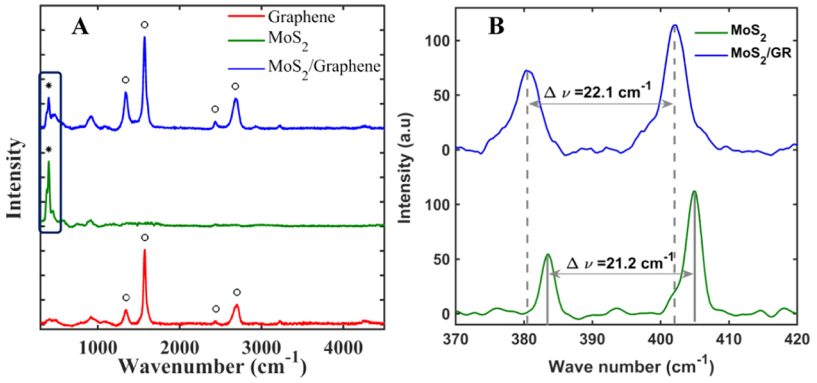

Figure 3. Micro-Raman spectra of liquid-phase exfoliated graphene (red line), MoS_2 (green line), and the MoS_2/graphene heterostructure in a 3:7 water/isopropanol mixture in a (A) wider scan range and a (B) high-resolution scan.

The quantitative amount of defects in the exfoliated graphene was estimated using Tuinstra−Koenig relation as follows[51,52]

$$L_a = (2.4 \times 10^{-10})\lambda^4 (I_D/I_G)^{-1} \quad (1)$$

where L_a is the in-plane crystallite size in nanometer and λ is the wavelength of the excitation source (532 nm in the present measurement). The estimated in-plane crystallite sizes were 97 and 48 nm for the exfoliated graphene and the MoS_2/graphene heterostructure, respectively. The translational symmetry of the graphene sheets was directly related to the presence of defects and structural disorders.[53] An increase in defects and/or disorders in the structure leads to a reduced in-plane crystallite size. The density of defects is calculated from the in-plane crystallite size using the following relation

$$n_D\,(\mathrm{cm}^{-2}) = 10^{14}/\pi L_a^2 \quad (2)$$

where n_D is the defect density and estimated to be 0.33×10^{10} and 1.34×10^{10} cm^{-2} for the exfoliated graphene and the MoS_2/graphene heterostructure, respectively. The decrease in the size of the in-plane crystallites and the higher defect density upon the formation of the heterostructure may be attributed to the effective exfoliation under the chosen solvent mixture and/or partial oxidation of graphene during ultrasonic treatment. The width of the "G" peak also implies the nature of defects and the presence of other impurities. In the present case, the observed width of ∼15 cm^{-1} for both exfoliated graphene and the MoS_2/graphene heterostructure implies that the material is almost equal to mechanically exfoliated graphene in purity. Such quality production of few-layered heterostructures is attributed to the usage of low-boiling and environmentally benign solvent mixtures during exfoliation.

Raman spectra of MoS_2 and the MoS_2/graphene heterostructure, shown in Figure 3A, have a peak at ∼400 cm^{-1} accompanied by a shoulder. To resolve the spectral signs of MoS_2, a narrow scan was carried out (Figure 3B), which clearly reveals peaks at 383.6 and 404.8 cm^{-1} with a peak separation of 21.2 cm^{-1}. Lattice vibrations and the intralayer bonding in stacked few-layered crystallites were perturbed by weak van der Waals interlayer interactions. The E_{2g} mode assigned to the opposite vibration of S atoms with respect to the Mo atom and the out-of-plane vibration of only S atoms in opposite directions yields the A_{1g} mode.[54] The layer thickness-dependent frequency shift of both modes has been examined, and the frequency of the E_{2g} peak decreases while that of the A_{1g} peak increases with increasing layer thickness.

In addition, the peak separation and the intensity of the peaks E_{2g} and A_{1g} increase with the increase in the number of layers.[15] The liquid exfoliated MoS_2 sample prepared by the present mixed-solvent method has a sheet with a thickness of two to four layers as evident from the frequencies of the A_{1g} and E_{2g} modes and the separation frequency of the two peaks. However, a shift in the peak position compared to the mechanically exfoliated sample may be attributed to the nature of the solvent/material interaction or partial oxidation of MoS_2 nanosheets. The peak frequencies of both E_{2g} and A_{1g} show a shift toward lower wavenumbers in the presence of graphene, which is ascribed to the constrained out-of-plane vibrations

https://doi.org/10.1021/acsomega.1c05250
ACS Omega 2022, 7, 629−637

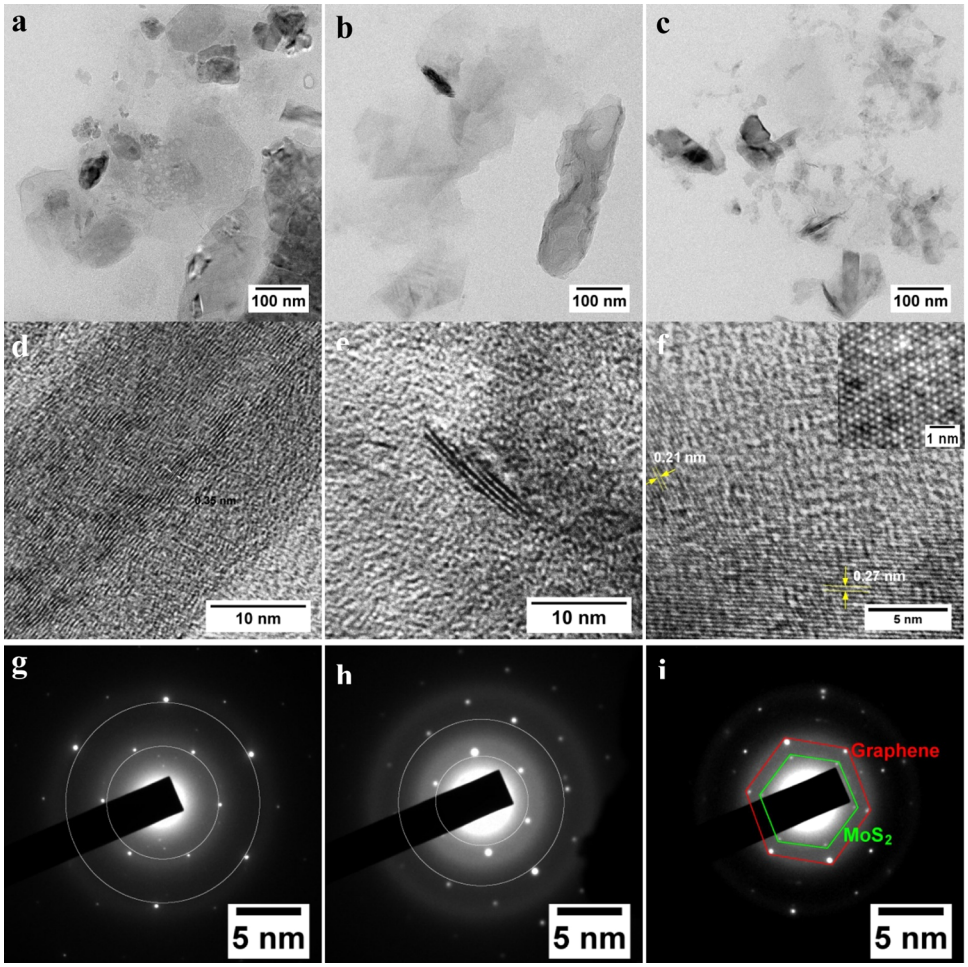

Figure 4. Transmission electron microscopy (TEM) images: (a, d) graphene, (b, e) MoS_2, and (c, f) the MoS_2/graphene heterostructure. Top panel: large-area scan and middle panel: high-resolution scan. SAED pattern of (g) graphene, (h) MoS_2, and (i) the MoS_2/graphene heterostructure.

due to the effective formation of the heterostructure. Also, every particle or position monitored during Raman measurement shows the features of both MoS_2 and graphene. This is a clear indication of the absence of free particles of both MoS_2 and graphene in the synthesized heterostructure. At present, the nature of interaction dominating the formation of the heterostructure is not clear. However, the balance between weak hydrogen bonding and hydrophobic and hydrophilic interaction might be the driving force for the effective formation of the heterostructure during liquid-phase exfoliation.

Structural Analysis of the Heterostructure. The size and lattice alignment of the MoS_2/graphene heterostructure were analyzed using transmission electron microscopy and small-angle electron diffraction as shown in Figure 4. A typical hexagonal diffraction pattern was seen in both MoS_2 and graphene SAED patterns with a lattice spacing of 0.67 and 0.35 nm, respectively.[55] The observed lattice spacing confirmed that the sonication-assisted liquid-phase exfoliation did not alter the interlayer distance as seen in some of the previous studies. The vertical stacking of the synthesized heterostructure is also evident from the high-resolution image shown in Figure 4f. Vertical heterostructures of TMDCs with graphene have been achieved with controlled chemical vapor deposition and mechanical exfoliation followed by transfer.[56,57] However, this is the first time vertical heterostructures of MoS_2/graphene were synthesized by single-stage, scalable liquid-phase exfoliation. Moreover, the position of the SAED pattern reveals that the angle of lattice orientation between graphene and MoS_2 might be either 0 or 60° in many cases, as we did not notice any other orientation angle in the SAED pattern. The characterizations carried out above unambiguously confirmed that the mixed-solvent liquid-phase exfoliation method adopted to synthesize heterostructures of MoS_2/graphene was effective, and the strategy is scalable for large-scale preparation of heterostructures with the advantage of the combined/modulated optical and electrical properties of both.

The photoluminescence behavior of MoS_2 in suspension and its heterostructure with graphene was evaluated by steady-state and time-resolved measurements. MoS_2 is a direct-band semiconductor, and the band-gap emission occurs at 1.9 eV (~650 nm) due to the interband transition of the K point.[47] This interband photoluminescence is observed at 688 nm for MoS_2 on excitation using 532 nm wavelength in suspension (Figure 5A). The mechanically exfoliated MoS_2 monolayer exhibits strong photoluminescence with a peak at 650−690 nm and a shoulder at around 610 nm due to A and B excitonic bands, respectively. The photoluminescence peak maximum of the monolayer and few layers shifts on different substrates such as sapphire, SiO_2, Si, and fused silica.[58] Moreover, the nature of

https://doi.org/10.1021/acsomega.1c05250
ACS Omega 2022, 7, 629−637

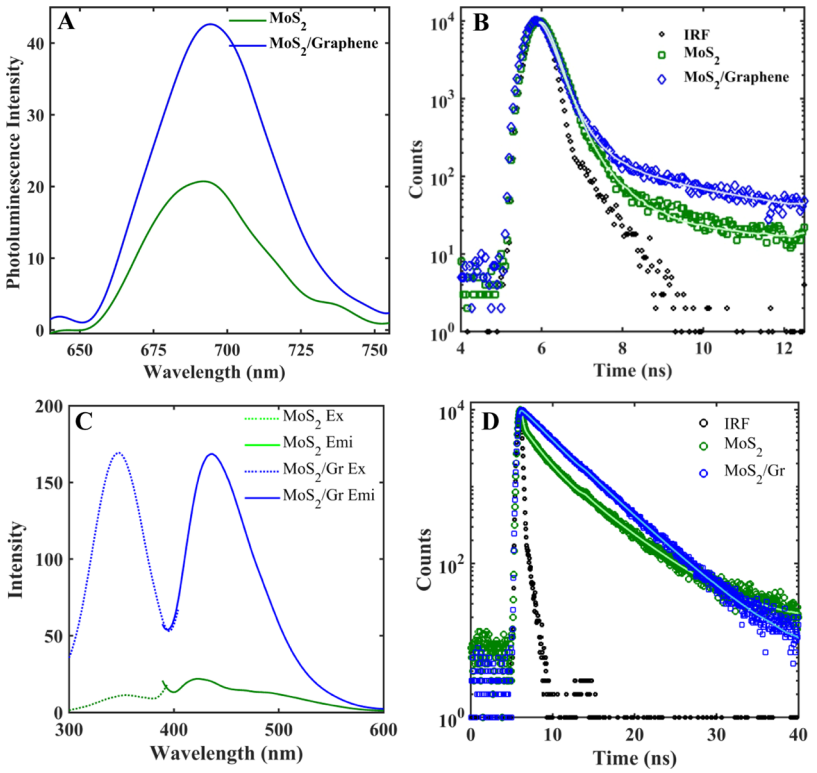

Figure 5. (A) Photoluminescence excitation (dotted line) and emission spectra (solid line) of MoS_2 (green line) and the MoS_2/graphene heterostructure in a 3:7 water/isopropanol mixture, (B, D) photoluminescence decay profile monitored at 450 and 680 nm on excitation at 375 and 470 nm wavelengths using picosecond laser diodes, respectively, and (C) photoluminescence emission spectra corresponding to the band-gap excitation measured by exciting with a 532 nm laser source.

impurities also plays a critical role in the photoluminescence intensity and peak position. Chemically exfoliated MoS_2 exhibits metallic behavior due to lithium intercalation under normal conditions and upon mild annealing results in the restoration of the intrinsic photoluminescence of the thin film.[47] In the present case, the observed photoluminescence slightly shifted to the red region, which may be due to solvent−solute interaction in the suspended MoS_2. However, the MoS_2/graphene heterostructure shows a peak maximum at 695 nm, which shows a further red shift compared to MoS_2 alone in the solvent system. Further, it is observed that the photoluminescence intensity increased to twice that of MoS_2 alone. This could be explained by the fact that interlayer coupling between MoS_2 and graphene results in an increase in layer thickness.

The photoluminescence intensity and the peak position depend on the layer thickness, and a red shift in the emission intensity is observed upon increasing the layer thickness.[47] On the other hand, the increase in the PL intensity may be attributed to the interlayer coupling of MoS_2 and graphene layers, which in turn reduces the rate of nonradiative decay.[59] Further, the photoluminescence behavior was analyzed by time-resolved PL decay as shown in Figure 5B and Table 1. The decay obeys a biexponential function with a prominent shorter decay time of 0.2 ns (95%) and a longer decay component of 4.0 ns (5%). The average decay time was estimated to be 0.4 ns. The MoS_2/graphene heterostructure also follows biexponential decay with decay times of 4.10 ns (10%) and 0.25 ns (90%), and the average lifetime was found to be 0.64 ns in the suspension. An average lifetime of 410 ps was reported by Mohamed et al. for the monolayer MoS_2, and the observed lifetime of 420 ps matches with their reports for MoS_2 suspension.[60] Moreover, the enhancement in decay time upon the formation of the heterostructure is consistent with the enhancement of luminescence intensity. This again validates that upon the formation of the heterostructure, the rate of nonradiative decay is decreased.

Table 1. Photoluminescence Parameters of Liquid-Phase Exfoliated MoS_2 and the MoS_2/Graphene Heterostructure[a]

sample	λ_{max} emission (nm)	decay time τ_1 (ns)	decay time τ_2 (ns)	$\langle\tau\rangle$ (ns)
MoS_2	430 (360)	5.35 (67)	1.95 (33)	4.23
	688 (532)	4.08 (5)	0.23 (95)	0.42
MoS_2/graphene	438 (355)	4.75 (71)	3.01 (29)	4.25
	695 (532)	4.10 (10)	0.25 (90)	0.64

[a]Excitation wavelength corresponding to the emission maximum is given in parentheses. Amplitudes for the respective decay times are given in parentheses.

Earlier, it was observed that the suspension of MoS_2 in solution exhibits strong luminescence in the blue region due to defect sites or size quantization in addition to band-edge emission.[61−63] The effect of the heterostructure on the photoluminescence properties of MoS_2 due to defect sites has also been explored. Figure 5C,D shows the steady-state and time-resolved photoluminescence of MoS_2 and the MoS_2/graphene heterostructure. Maximum photoluminescence intensity was observed upon excitation at 360 nm with a peak at 430 nm, and the respective excitation spectrum is also shown in Figure 5C. MoS_2 sheets exhibit excitation-dependent

https://doi.org/10.1021/acsomega.1c05250
ACS Omega 2022, 7, 629−637

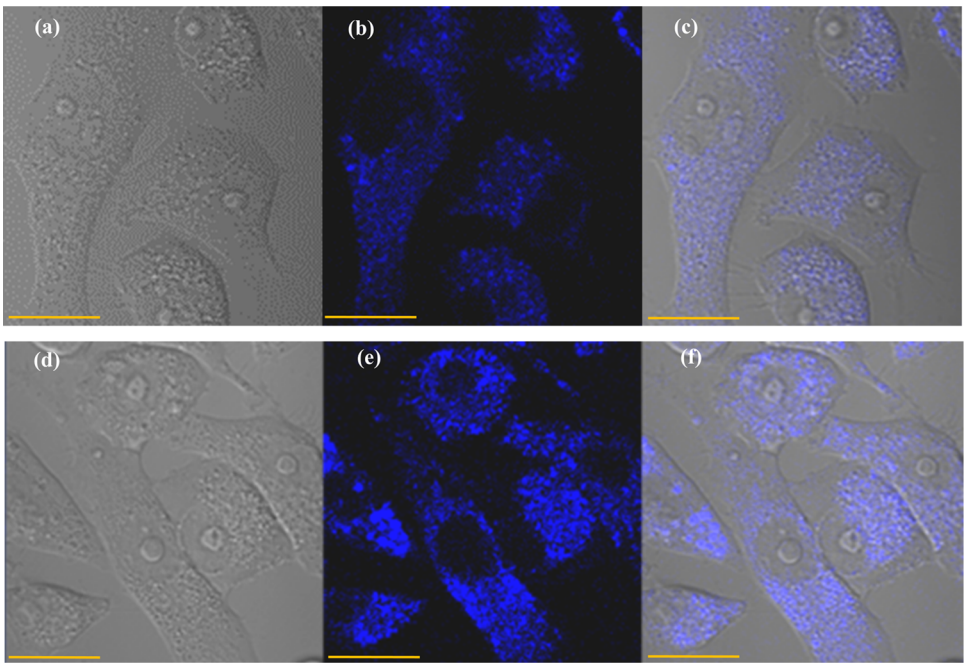

Figure 6. (a, d) Bright-field images, (b, e) fluorescence images, and (c, f) merged images of HeLa cells incubated for 1 h in MoS_2 and the MoS_2/graphene heterostructure in PBS buffer.

emission in the blue region attributed to inhomogeneous size distribution and the presence of multiple trap states.[43,61]

Interestingly, more than 20-fold enhancement in the emission intensity was observed for the heterostructure, as seen in Figure 5C. This may be due to the combined effect of an increase in the number of defect sites and the reduction in the nonradiative rate in the heterostructure. This is further ascertained by measuring the time-resolved decay profile as shown in Figure 5D. The decay profile displays a biexponential decay with decay times of 5.3 ns (67%) and 1.95 ns (33%) for MoS_2. The average decay times were estimated to be 4.23 and 4.25 ns for MoS_2 and the MoS_2/graphene heterostructure, respectively. The nearly identical decay time for both and an enhancement in the PL intensity may be correlated to the increase in defect sites upon the heterostructure formation.

The effect of MoS_2 on normal and cancer cell lines has been studied earlier, and the results indicate that MoS_2 adhesion leads to cell death in cancerous cell lines and has no effect on the normal cell lines after 24 h of incubation.[18] The uptake of MoS_2 and its localization inside the cell is probed using transient absorption and Raman scattering in a custom-built dual-mode microscope using HeLa cell lines.[64] However, live-cell imaging using MoS_2 as a luminescent probe is limited due to the poor photoluminescence of the material in biological medium.[61,65] The heterostructure obtained by the present strategy has more than 20-fold enhancement in luminescence intensity compared to MoS_2 nanosheets under identical conditions and might be a potential candidate for live-cell imaging using the photoluminescence of the material. HeLa cell lines incubated with 50 mL of the resuspended MoS_2/graphene heterostructure were used for imaging as mentioned in the Materials and Methods section in a biological buffer medium (Figure 6). Bright-field images of the cells incubated with 50 μL of the redispersed MoS_2 and its heterostructure are shown in Figure 6a,d, and it is noticed that the cells are alive up to 12 h in the incubated medium. Fluorescent and merged images of the cells reveal that both the materials internalized into the cytoplasm of the cells. In addition, it is clearly visible that the heterostructure has an enhanced fluorescent contrast compared to MoS_2 alone in an identical environment.

CONCLUSIONS

The heterostructure of MoS_2 with graphene was successfully fabricated by single-stage liquid-phase exfoliation using an IPA/water mixture (7:3 v/v). Thus, the obtained van der Waals heterostructure was characterized using Raman, UV−visible, TEM, and dynamic light scattering studies. The heterostructures have two to five layers of MoS_2 as evident from Raman and UV−visible analyses. DLS, UV−visible, and TEM analyses revealed that the lateral size of the material was about 200 nm and the surface of both MoS_2 and the heterostructure was negatively charged with ζ-potential values of ∼−60 mV. TEM with SAED confirm the formation of the vertical heterostructure of MoS_2/graphene with the present strategy. About 20-fold enhancement in the photoluminescence intensity was attributed to the suppression of nonradiative decay pathways due to the formation of the heterostructure, which is also clear from higher decay times in time-resolved photoluminescence measurement. The material shows a potential application in live-cell imaging using photoluminescence compared to MoS_2 with the added advantage of graphene in the heterostructure.

MATERIALS AND METHODS

Synthesis of the MoS_2/Graphene Heterostructure. HOPG and MoS_2 crystals used in this work were purchased from 2D Semiconductors. All other reagents were of analytical grade and used as received. Millipore water was used throughout the study. The individually exfoliated materials were prepared following the methods described earlier.[46] The heterostructure was synthesized by slightly modifying the above protocol (Figure 1). Briefly, 5 mg of graphene and MoS_2 were taken in a mortar and ground into a powder. Then, the

https://doi.org/10.1021/acsomega.1c05250
ACS Omega 2022, 7, 629−637

contents were transferred to a glass vial and sonicated for 1 h in a 3:7 v/v water/IPA mixture. The resultant suspension was centrifuged at 2000 rpm for 10 min, and the supernatant was used for further characterization and studies.

Characterization of the MoS_2/Graphene Heterostructure. Absorption spectra for the suspensions at room temperature were recorded on a Shimadzu 2401 UV−visible spectrophotometer with a spectral range of 250−1100 nm. Micro-Raman analysis at room temperature was carried out on individual sheets drop-cast on a precleaned borosilicate coverslip. The spectrographs were recorded using a BLZE-100 HR EMCCD camera (Princeton Instruments) equipped with an Acton SP2500 monochromator and a confocal microscope. A 532 nm continuous-wave, tunable power laser was used for excitation through a 60× objective. The lateral size and ζ-potential of the exfoliated samples were recorded using a Horiba Nanopartica SZ-100 instrument by dynamic light scattering and ζ-potential measurement, respectively. Transmission electron microscopy images with small-angle electron diffraction were recorded for the samples coated on a copper grid and dried in vacuum using a JEOL-2100 + high-resolution transmission electron microscope. Confocal fluorescence images were acquired with a Zeiss LSM 710 under the excitation wavelength of 405 nm.

Photoluminescence Studies of the MoS_2/Graphene Heterostructure. Photoluminescence emission and excitation spectra were recorded on a Horiba−Jobin Yvon FluoroMax-4P spectrofluorometer equipped with a Xe lamp for excitation and an R928P photon counting module for the detection of light emitted from the sample. The emission from the direct-band-gap excitation was monitored using a 5 mW, 532 nm CW laser as the excitation source and a USB spectrometer (RI Instruments and Innovation, India). Photoluminescence decay was monitored using the TCSPC technique (Model 5000U, IBH, U.K.) and a 375 nm, picosecond pulse LED as the excitation source, and an MCP-PMT (Hamamatsu R3809U) was used for detection of photons emitted after passing through a monochromator. The decay was fitted with Horiba Scientific decay analysis software DAS6 to a bi/triexponential behavior.

In Vitro Fluorescence Bioimaging. HeLa cells were obtained from American Type Culture Collection and cultured in RPMI-1640 medium supplemented with FBS (10%), antibiotic-antimycotic solution (1%), L-glutamine (2 mM), and nonessential amino acids (1%). The live cells were maintained at 37 °C and 5% CO_2 in a humidified chamber. HeLa cells were incubated with MoS_2 (50 μL) for 30 min to equilibrate the experimental conditions. After incubation, the cells were washed with PBS buffer to remove extracellular MoS_2 prior to recording images. The fluorescence images of MoS_2 and the MoS_2/graphene heterostructure incubated cells were recorded at the excitation wavelength of 405 nm with confocal fluorescence microscopy.

AUTHOR INFORMATION

Corresponding Author

Durai Murugan Kandhasamy − *Department of Bioelectronics and Biosensors, Alagappa University, Karaikudi 630003 Tamil Nadu, India;* orcid.org/0000-0003-2925-4728; Email: kdmurugan@gmail.com

Authors

Paulpandian Muthu Mareeswaran − *Department of Industrial Chemistry, Alagappa University, Karaikudi 630003 Tamil Nadu, India;* orcid.org/0000-0002-2901-4110

Selvaraju Chellappan − *National Centre for Ultrafast Processes, University of Madras, Chennai 600113, India;* orcid.org/0000-0002-3625-4243

Dhenadhayalan Namasivayam − *Department of Chemistry, National Taiwan University and Institute of Atomic and Molecular Sciences, Academia Sinica, Taipei 10617, Taiwan;* orcid.org/0000-0003-4494-5746

Afaf Aldahish − *Department of Pharmacology, School of Pharmacy, King Khalid University, Abha 62529, Saudi Arabia*

Kumarappan Chidambaram − *Department of Pharmacology, School of Pharmacy, King Khalid University, Abha 62529, Saudi Arabia*

Complete contact information is available at: https://pubs.acs.org/10.1021/acsomega.1c05250

Notes

The authors declare no competing financial interest.

ACKNOWLEDGMENTS

D.M.K. and M.M.P. acknowledge the financial support from RUSA 2.0 (MHRD-India) grant sanctioned vide Letter No. F. 24-51/2014-U, Policy (TNMulti-Gen), Department of Education, Government of India, dated October 09, 2018. One of the author K.C. would like to thank the Deanship of Scientific Research (RGP: 1/275/1442), King Khalid University, Abha, Suadi Arabia.

REFERENCES

(1) Wang, Q. H.; Kalantar-Zadeh, K.; Kis, A.; Coleman, J. N.; Strano, M. S. Electronics and Optoelectronics of Two-Dimensional Transition Metal Dichalcogenides. *Nat. Nanotechnol.* **2012**, *7*, 699−712.

(2) Chhowalla, M.; Shin, H. S.; Eda, G.; Li, L. J.; Loh, K. P.; Zhang, H. The Chemistry of Two-Dimensional Layered Transition Metal Dichalcogenide Nanosheets. *Nat. Chem.* **2013**, *5*, 263−275.

(3) Weng, M.; Li, S.; Zheng, J.; Pan, F.; Wang, L. W. Wannier Koopmans Method Calculations of 2D Material Band Gaps. *J. Phys. Chem. Lett.* **2018**, *9*, 281−285.

(4) Yadav, V.; Roy, S.; Singh, P.; Khan, Z.; Jaiswal, A. 2D MoS_2-Based Nanomaterials for Therapeutic, Bioimaging, and Biosensing Applications. *Small* **2019**, *15*, No. 1803706.

(5) Backes, C.; Smith, R. J.; McEvoy, N.; Berner, N. C.; McCloskey, D.; Nerl, H. C.; O'Neill, A.; King, P. J.; Higgins, T.; Hanlon, D.; et al. Edge and Confinement Effects Allow in Situ Measurement of Size and Thickness of Liquid-Exfoliated Nanosheets. *Nat. Commun.* **2014**, *5*, No. 4576.

(6) Zhang, W.; Zhang, P.; Su, Z.; Wei, G. Synthesis and Sensor Applications of MoS_2 -Based Nanocomposites. *Nanoscale* **2015**, *7*, 18364−18378.

(7) Papanai, G. S.; Sharma, I.; Kedawat, G.; Gupta, B. K. Qualitative Analysis of Mechanically Exfoliated MoS_2 Nanosheets Using Spectroscopic Probes. *J. Phys. Chem. C* **2019**, *123*, 27264−27271.

(8) Nerl, H. C.; Winther, K. T.; Hage, F. S.; Thygesen, K. S.; Houben, L.; Backes, C.; Coleman, J. N.; Ramasse, Q. M.; Nicolosi, V. Probing the Local Nature of Excitons and Plasmons in Few-Layer MoS_2. *npj 2D Mater. Appl.* **2017**, *1*, No. 2.

(9) Khan, M. M. *Chalcogenide-Based Nanomaterials as Photocatalysts*; Elsevier Inc., 2021.

(10) Kalantar-Zadeh, K.; Ou, J. Z. Biosensors Based on Two-Dimensional MoS_2. *ACS Sens.* **2016**, *1*, 5−16.
(11) Rao, K. S.; Senthilnathan, J.; Liu, Y. F.; Yoshimura, M. Role of Peroxide Ions in Formation of Graphene Nanosheets by Electrochemical Exfoliation of Graphite. *Sci. Rep.* **2014**, *4*, No. 4237.
(12) Yang, H.; Withers, F.; Gebremedhn, E.; Lewis, E.; Britnell, L.; Felten, A.; Palermo, V.; Haigh, S.; Beljonne, D.; Casiraghi, C. Dielectric Nanosheets Made by Liquid-Phase Exfoliation in Water and Their Use in Graphene-Based Electronics. *2D Mater.* **2014**, *1*, No. 011012.
(13) Gao, Y.; Shi, W.; Wang, W.; Wang, Y.; Zhao, Y.; Lei, Z.; Miao, R. Ultrasonic-Assisted Production of Graphene with High Yield in Supercritical CO_2 and Its High Electrical Conductivity Film. *Ind. Eng. Chem. Res.* **2014**, *53*, 2839−2845.
(14) Wu, J. B.; Lin, M. L.; Cong, X.; Liu, H. N.; Tan, P. H. Raman Spectroscopy of Graphene-Based Materials and Its Applications in Related Devices. *Chem. Soc. Rev.* **2018**, *47*, 1822−1873.
(15) Lee, C.; Yan, H.; Brus, L. E.; Heinz, T. F.; Hone, J.; Ryu, S. Anomalous Lattice Vibrations of Single- and Few-Layer MoS_2. *ACS Nano* **2010**, *4*, 2695−2700.
(16) Koitzsch, A.; Pawlik, A. S.; Habenicht, C.; Klaproth, T.; Schuster, R.; Büchner, B.; Knupfer, M. Nonlocal Dielectric Function and Nested Dark Excitons in MoS_2. *npj 2D Mater. Appl.* **2019**, *3*, No. 41.
(17) Wang, Q.; Huang, J.; Sun, H.; Ng, Y. H.; Zhang, K. Q.; Lai, Y. MoS_2 Quantum Dots@TiO_2 Nanotube Arrays: An Extended-Spectrum-Driven Photocatalyst for Solar Hydrogen Evolution. *ChemSusChem* **2018**, *11*, 1708−1721.
(18) Kaur, J.; Singh, M.; Dell'Aversana, C.; Benedetti, R.; Giardina, P.; Rossi, M.; Valadan, M.; Vergara, A.; Cutarelli, A.; Montone, A. M. I.; et al. Biological Interactions of Biocompatible and Water-Dispersed MoS_2 Nanosheets with Bacteria and Human Cells. *Sci. Rep.* **2018**, *8*, No. 16386.
(19) Khan, M. E.; Khan, M. M.; Cho, M. H. CdS-Graphene Nanocomposite for Efficient Visible-Light-Driven Photocatalytic and Photoelectrochemical Applications. *J. Colloid Interface Sci.* **2016**, *482*, 221−232.
(20) Faridi, E.; Moradi, M.; Ansari, N.; Ghasemi, A. H. B.; Afshar, A.; Mohseni, S. M. Au/NiFe/M(Au, MoS_2, Graphene) Trilayer Magnetoplasmonics DNA-Hybridized Sensors with High Record of Sensitivity. *J. Biomed. Opt.* **2017**, *22*, 1.
(21) Li, X.; Guo, S.; Li, W.; Ren, X.; Su, J.; Song, Q.; Sobrido, A. J.; Wei, B. Edge-Rich MoS_2 Grown on Edge-Oriented Three-Dimensional Graphene Glass for High-Performance Hydrogen Evolution. *Nano Energy* **2019**, *57*, 388−397.
(22) Mukherjee, S.; Maiti, R.; Katiyar, A. K.; Das, S.; Ray, S. K. Novel Colloidal MoS_2 Quantum Dot Heterojunctions on Silicon Platforms for Multifunctional Optoelectronic Devices. *Sci. Rep.* **2016**, *6*, No. 29016.
(23) Naz, R.; Imtiaz, M.; Liu, Q.; Yao, L.; Abbas, W.; Li, T.; Zada, I.; Yuan, Y.; Chen, W.; Gu, J. Highly Defective 1T-MoS_2 Nanosheets on 3D Reduced Graphene Oxide Networks for Supercapacitors. *Carbon* **2019**, *152*, 697−703.
(24) Sahoo, P. K.; Memaran, S.; Nugera, F. A.; Xin, Y.; Díaz Márquez, T.; Lu, Z.; Zheng, W.; Zhigadlo, N. D.; Smirnov, D.; Balicas, L.; et al. Bilayer Lateral Heterostructures of Transition-Metal Dichalcogenides and Their Optoelectronic Response. *ACS Nano* **2019**, *13*, 12372−12384.
(25) Xiao, R.; Lan, C.; Li, Y.; Zeng, C.; He, T.; Wang, S.; Li, C.; Yin, Y.; Liu, Y. High Performance Van Der Waals Graphene−WS_2−Si Heterostructure Photodetector. *Adv. Mater. Interfaces* **2019**, *6*, No. 1901304.
(26) Luo, Y. K.; Xu, J.; Zhu, T.; Wu, G.; McCormick, E. J.; Zhan, W.; Neupane, M. R.; Kawakami, R. K. Opto-Valleytronic Spin Injection in Monolayer MoS_2/Few-Layer Graphene Hybrid Spin Valves. *Nano Lett.* **2017**, *17*, 3877−3883.
(27) Zheng, G.; Zou, X.; Chen, Y.; Xu, L.; Rao, W. Fano Resonance in Graphene-MoS_2 Heterostructure-Based Surface Plasmon Resonance Biosensor and Its Potential Applications. *Opt. Mater.* **2017**, *66*, 171−178.
(28) Xu, L.; Huang, W. Q.; Hu, W.; Yang, K.; Zhou, B. X.; Pan, A.; Huang, G. F. Two-Dimensional MoS_2-Graphene-Based Multilayer van Der Waals Heterostructures: Enhanced Charge Transfer and Optical Absorption, and Electric-Field Tunable Dirac Point and Band Gap. *Chem. Mater.* **2017**, *29*, 5504−5512.
(29) Romanov, R. I.; Slavich, A. S.; Kozodaev, M. G.; Myakota, D. I.; Lebedinskii, Y. Y.; Novikov, S. M.; Markeev, A. M. Band Alignment in As-Transferred and Annealed Graphene/MoS_2 Heterostructures. *Phys. Status Solidi RRL* **2019**, *14*, No. 1900406.
(30) Zhou, Y.; Yang, Y.; Guo, Y.; Wang, Q.; Yan, X. Influence of Length and Interface Structure on Electron Transport Properties of Graphene-MoS_2 in-Plane Heterojunction. *Appl. Surf. Sci.* **2019**, *497*, No. 143764.
(31) Miwa, J. A.; Dendzik, M.; Grønborg, S. S.; Bianchi, M.; Lauritsen, J. V.; Hofmann, P.; Ulstrup, S. Van Der Waals Epitaxy of Two-Dimensional MoS_2-Graphene Heterostructures in Ultrahigh Vacuum. *ACS Nano* **2015**, *9*, 6502−6510.
(32) Rathi, S.; Lee, I.; Lim, D.; Wang, J.; Ochiai, Y.; Aoki, N.; Watanabe, K.; Taniguchi, T.; Lee, G. H.; Yu, Y. J.; et al. Tunable Electrical and Optical Characteristics in Monolayer Graphene and Few-Layer MoS_2 Heterostructure Devices. *Nano Lett.* **2015**, *15*, 5017−5024.
(33) Zhang, Y.; Shi, J.; Liu, M.; Wen, J.; Ren, X.; Zhou, X.; Ji, Q.; Ma, D.; Zhang, Y.; Jin, C.; et al. All Chemical Vapor Deposition Synthesis and Intrinsic Bandgap Observation of MoS_2/Graphene Heterostructures. *Adv. Mater.* **2015**, *27*, 7086−7092.
(34) Fu, W.; Du, F. H.; Su, J.; Li, X. H.; Wei, X.; Ye, T. N.; Wang, K. X.; Chen, J. S. In Situ Catalytic Growth of Large-Area Multilayered Graphene/MoS_2 Heterostructures. *Sci. Rep.* **2014**, *4*, No. 4673.
(35) Pandey, A.; Mukherjee, A.; Chakrabarty, S.; Chanda, D.; Basu, S. Interface Engineering of an RGO/MoS_2/Pd 2D Heterostructure for Electrocatalytic Overall Water Splitting in Alkaline Medium. *ACS Appl. Mater. Interfaces* **2019**, *11*, 42094−42103.
(36) Han, J.; Yan, T.; Shen, J.; Shi, L.; Zhang, J.; Zhang, D. Capacitive Deionization of Saline Water by Using MoS_2-Graphene Hybrid Electrodes with High Volumetric Adsorption Capacity. *Environ. Sci. Technol.* **2019**, *53*, 12668−12676.
(37) Zhao, P.; Ni, M.; Xu, Y.; Wang, C.; Chen, C.; Zhang, X.; Li, C.; Xie, Y.; Fei, J. A Novel Ultrasensitive Electrochemical Quercetin Sensor Based on MoS_2 - Carbon Nanotube @ Graphene Oxide Nanoribbons/HS-Cyclodextrin/Graphene Quantum Dots Composite Film. *Sens., Actuators, B* **2019**, *299*, No. 126997.
(38) Kim, Y.; Choi, D.; Woo, W. J.; Lee, J. B.; Ryu, G. H.; Lim, J. H.; Lee, S.; Lee, Z.; Im, S.; Ahn, J. H.; et al. Synthesis of Two-Dimensional MoS_2/Graphene Heterostructure by Atomic Layer Deposition Using MoF6 Precursor. *Appl. Surf. Sci.* **2019**, *494*, 591−599.
(39) Hou, L.; Zhang, Q.; Tweedie, M.; Shautsova, V.; Sheng, Y.; Zhou, Y.; Huang, H.; Chen, T.; Warner, J. H. Photocurrent Direction Control and Increased Photovoltaic Effects in All-2D Ultrathin Vertical Heterostructures Using Asymmetric h-BN Tunneling Barriers. *ACS Appl. Mater. Interfaces* **2019**, *11*, 40274−40282.
(40) Dong, L.; Lin, S.; Yang, L.; Zhang, J.; Yang, C.; Yang, D.; Lu, H. Spontaneous Exfoliation and Tailoring of MoS_2 in Mixed Solvents. *Chem. Commun.* **2014**, *50*, 15936−15939.
(41) Jawaid, A.; Nepal, D.; Park, K.; Jespersen, M.; Qualley, A.; Mirau, P.; Drummy, L. F.; Vaia, R. A. Mechanism for Liquid Phase Exfoliation of MoS_2. *Chem. Mater.* **2016**, *28*, 337−348.
(42) Xu, Y.; Cao, H.; Xue, Y.; Li, B.; Cai, W. Liquid-Phase Exfoliation of Graphene: An Overview on Exfoliation Media, Techniques, and Challenges. *Nanomaterials* **2018**, *8*, No. 942.
(43) Wu, J. Y.; Zhang, X. Y.; Ma, X. D.; Qiu, Y. P.; Zhang, T. High Quantum-Yield Luminescent MoS_2 Quantum Dots with Variable Light Emission Created via Direct Ultrasonic Exfoliation of MoS_2 Nanosheets. *RSC Adv.* **2015**, *5*, 95178−95182.
(44) Geim, A. K.; Grigorieva, I. V. Van Der Waals Heterostructures. *Nature* **2013**, *499*, 419−425.

https://doi.org/10.1021/acsomega.1c05250
ACS Omega 2022, 7, 629−637

(45) Shen, J.; He, Y.; Wu, J.; Gao, C.; Keyshar, K.; Zhang, X.; Yang, Y.; Ye, M.; Vajtai, R.; Lou, J.; et al. Liquid Phase Exfoliation of Two-Dimensional Materials by Directly Probing and Matching Surface Tension Components. *Nano Lett.* **2015**, *15*, 5449−5454.
(46) Bernal, M. M.; Álvarez, L.; Giovanelli, E.; Arnáiz, A.; Ruiz-González, L.; Casado, S.; Granados, D.; Pizarro, A. M.; Castellanos-Gomez, A.; Pérez, E. M. Luminescent Transition Metal Dichalcogenide Nanosheets through One-Step Liquid Phase Exfoliation. *2D Mater.* **2016**, *3*, No. 035014.
(47) Eda, G.; Yamaguchi, H.; Voiry, D.; Fujita, T.; Chen, M.; Chhowalla, M. Photoluminescence from Chemically Exfoliated MoS_2. *Nano Lett.* **2011**, *11*, 5111−5116.
(48) Klots, A. R.; Newaz, A. K. M.; Wang, B.; Prasai, D.; Krzyzanowska, H.; Lin, J.; Caudel, D.; Ghimire, N. J.; Yan, J.; Ivanov, B. L.; et al. Probing Excitonic States in Suspended Two-Dimensional Semiconductors by Photocurrent Spectroscopy. *Sci. Rep.* **2014**, *4*, No. 6608.
(49) Konkena, B.; Vasudevan, S. Understanding Aqueous Dispersibility of Graphene Oxide and Reduced Graphene Oxide through pKa Measurements. *J. Phys. Chem. Lett.* **2012**, *3*, 867−872.
(50) Yadgarov, L.; Choi, C. L.; Sedova, A.; Cohen, A.; Rosentsveig, R.; Bar-Elli, O.; Oron, D.; Dai, H.; Tenne, R. Dependence of the Absorption and Optical Surface Plasmon Scattering of MoS_2 Nanoparticles on Aspect Ratio, Size, and Media. *ACS Nano* **2014**, *8*, 3575−3583.
(51) Tuinstra, F.; Koenig, J. L. Raman Spectrum of Graphite. *J. Chem. Phys.* **1970**, *53*, 1126−1130.
(52) Cançado, L. G.; Jorio, A.; Ferreira, E. H. M.; Stavale, F.; Achete, C. A.; Capaz, R. B.; Moutinho, M. V. O.; Lombardo, A.; Kulmala, T. S.; Ferrari, A. C. Quantifying Defects in Graphene via Raman Spectroscopy at Different Excitation Energies. *Nano Lett.* **2011**, *11*, 3190−3196.
(53) Backes, C.; Abdelkader, A. M.; Alonso, C.; et al. Production and Processing of Graphene and Related Materials. *2D Mater.* **2020**, *7*, No. 022001.
(54) Wu, P. R.; Liu, Z.; Cheng, Z. L. Hydrothermal-Assisted Shearing Exfoliation for Few-Layered MoS_2 Nanosheets. *RSC Adv.* **2019**, *9*, 17016−17024.
(55) Liao, M.; Wu, Z. W.; Du, L.; Zhang, T.; Wei, Z.; Zhu, J.; Yu, H.; Tang, J.; Gu, L.; Xing, Y.; et al. Twist Angle-Dependent Conductivities across MoS_2/Graphene Heterojunctions. *Nat. Commun.* **2018**, *9*, No. 4068.
(56) Shi, J.; Zhou, X.; Han, G. F.; Liu, M.; Ma, D.; Sun, J.; Li, C.; Ji, Q.; Zhang, Y.; Song, X.; et al. Narrow-Gap Quantum Wires Arising from the Edges of Monolayer MoS_2 Synthesized on Graphene. *Adv. Mater. Interfaces* **2016**, *3*, No. 1600332.
(57) Safeer, C. K.; Ingla-Aynés, J.; Herling, F.; Garcia, J. H.; Vila, M.; Ontoso, N.; Calvo, M. R.; Roche, S.; Hueso, L. E.; Casanova, F. Room-Temperature Spin Hall Effect in Graphene/MoS_2 van Der Waals Heterostructures. *Nano Lett.* **2019**, *19*, 1074−1082.
(58) Mohapatra, P. K.; Deb, S.; Singh, B. P.; Vasa, P.; Dhar, S. Strictly Monolayer Large Continuous MoS_2 Films on Diverse Substrates and Their Luminescence Properties. *Appl. Phys. Lett.* **2016**, *108*, No. 042101.
(59) Palummo, M.; Bernardi, M.; Grossman, J. C. Exciton Radiative Lifetimes in Two-Dimensional Transition Metal Dichalcogenides. *Nano Lett.* **2015**, *15*, 2794−2800.
(60) Mohamed, N. B.; Lim, H. E.; Wang, F.; Koirala, S.; Mouri, S.; Shinokita, K.; Miyauchi, Y.; Matsuda, K. Long Radiative Lifetimes of Excitons in Monolayer Transition-Metal Dichalcogenides MX_2 (M = Mo, W; X = S, Se). *Appl. Phys. Express* **2018**, *11*, No. 015201.
(61) Zhou, K.; Zhang, Y.; Xia, Z.; Wei, W. As-Prepared MoS_2 Quantum Dot as a Facile Fluorescent Probe for Long-Term Tracing of Live Cells. *Nanotechnology* **2016**, *27*, No. 275101.
(62) Wang, N.; Wei, F.; Qi, Y.; Li, H.; Lu, X.; Zhao, G.; Xu, Q. Synthesis of Strongly Fluorescent Molybdenum Disulfide Nanosheets for Cell-Targeted Labeling. *ACS Appl. Mater. Interfaces* **2014**, *6*, 19888−19894.
(63) Wu, J. Y.; Lin, M. N.; Wang, L.-D.; Zhang, T. Photoluminescence of MoS_2 Prepared by Effective Grinding-Assisted Sonication Exfoliation. *J. Nanomater.* **2014**, *2014*, No. 852735.
(64) Zhang, L.; Shen, S.; Liu, Z.; Ji, M. Label-Free, Quantitative Imaging of MoS_2 -Nanosheets in Live Cells with Simultaneous Stimulated Raman Scattering and Transient Absorption Microscopy. *Adv. Biosyst.* **2017**, *1*, No. 1700013.
(65) Feng, W.; Chen, L.; Qin, M.; Zhou, X.; Zhang, Q.; Miao, Y.; Qiu, K.; Zhang, Y.; He, C. Flower-like PEGylated MoS_2 Nanoflakes for near-Infrared Photothermal Cancer Therapy. *Sci. Rep.* **2015**, *5*, No. 17422.

https://doi.org/10.1021/acsomega.1c05250
ACS Omega 2022, 7, 629−637